

Imaging Evaluation of Mediastinal Masses in Children and Adults

Practical Diagnostic Approach Based on A New Classification System

Paul G. Thacker, MD, Maryam G. Mahani, MD,† Amer Heider, MD,‡ and Edward Y. Lee, MD, MPH§*

Abstract: A compartmental approach to the diagnosis of the mediastinal masses in children and adults has been widely used to facilitate the diagnosis and planning of diagnostic interventions and surgical treatment for many years. Recently, a new computed tomography–based mediastinal division scheme, approved by the International Thymic Malignancy Interest Group, has received considerable attention as a potential new standard. In this review article, this new computed tomography–based mediastinal division scheme is described and illustrated. In addition, currently used imaging modalities and techniques, practical imaging algorithm of evaluating mediastinal masses, and characteristic imaging findings of various mediastinal masses that occur in children and adults are discussed. Such up-to-date knowledge has the potential to facilitate better understanding of mediastinal masses in both pediatric and adult populations.

Key Words: mediastinum, radiography, ultrasound, computed tomography, magnetic resonance imaging

(*J Thorac Imaging* 2015;30:247–267)

LEARNING OBJECTIVES

After completing this SAM-CME activity, physicians should be better able to:

1. Localize mediastinal masses based on the updated ITMIG CT-based mediastinal classification scheme.
2. Provide a succinct differential diagnosis based on mediastinal compartment.
3. Accurately characterize the most common imaging findings for pediatric and adult mediastinal masses.
4. Recommend the best imaging modality available for assessment of mediastinal masses based on compartmental location and patient age.

*Assistant Professor, Department of Radiology and Radiological Science, Medical University of South Carolina, Charleston, SC;

†Assistant Professor, Department of Radiology, Division of Cardiothoracic Radiology and Section of Pediatric Radiology, University of Michigan, C.S. Mott Children's Hospital; ‡Assistant Professor of Pathology, Department of Pathology, University of Michigan Health System, Ann Arbor, MI; and §Chief, Division of Thoracic Imaging, Department of Radiology, Boston Children's Hospital and Harvard Medical School, Boston, MA.

All authors and staff in a position to control the content of this CME activity and their spouses/life partners (if any) have disclosed that they have no financial relationships with, or financial interests in, any commercial organization pertaining to this education activity.

Correspondence to: Paul Thacker, MD, Department of Radiology and Radiological Science, 96 Jonathon Lucas Street MSC 323, Charleston, SC 29425 (e-mail: thackerp@musc.edu).

Copyright © 2015 Wolters Kluwer Health, Inc. All rights reserved.

 DOI: 10.1097/RTI.0000000000000161

The mediastinum comprises the thoracic compartment bounded by the thoracic inlet superiorly, the diaphragm inferiorly, the posterior sternal border anteriorly, and posteriorly by the vertebral column.^{1,2} Over the years, multiple compartmental classification schemes have been developed, traditionally based on lateral radiograph anatomy. However, traditional schemes largely split the mediastinum on the basis of arbitrary and nonanatomic divisions. With increased multidetector computed tomography (MDCT) usage, the diagnosis and treatment of mediastinal lesions has nearly completely shifted from chest radiography (CR) to MDCT. Thus, a new classification system for dividing the mediastinum is warranted and has recently been brought forth in the medical literature.^{3,4}

In 2014, the Japanese Association of Research of the Thymus was the first group to propose a CT-based mediastinal classification system. Here, the authors performed a retrospective review of 445 pathologically proven mediastinal lesions, proposing a CT-based 4-compartment model.³ This 4-compartment model is advantageous given its similarities to other established radiologic and anatomic 4-compartment models, its efficacy as the Japanese Association of Research of the Thymus group demonstrated, and its recognition that thyroid goiters primarily remain confined within the superior mediastinum. Disadvantages relate to the added complexity of having a fourth compartment, nonanatomic features of the 4-compartment scheme, and the overall perception within the medical community of the lack of usage by clinicians and radiologist of the existing 4-compartment paradigms.⁴

Considering these factors, the International Thymic Malignancy Interest Group (ITMIG) sought to develop and recently published a CT-based 3-compartment mediastinal classification system. Here, 45 experts across several disciplines were surveyed with results finding that 72% preferred a 3-compartmental CT-based classification system. Sixty-seven percent believed that such a system would lead to optimal disease entity distinction. Ultimately, the ITMIG proposed mediastinal division into prevascular (anterior), visceral (middle), and paravertebral (posterior) compartments (Fig. 1).⁴

The prevascular compartment is located anteriorly within the chest, and its major contents are the thymus, lymph nodes, mediastinal fat, and the left brachiocephalic vein. It is bounded by the thoracic inlet superiorly and the diaphragm inferiorly. Laterally, the prevascular compartment is demarcated by the mediastinal parietal pleural reflections, the inferior and superior pulmonary veins, and the bilateral internal thoracic artery and vein. The posterior cortex of the sternum

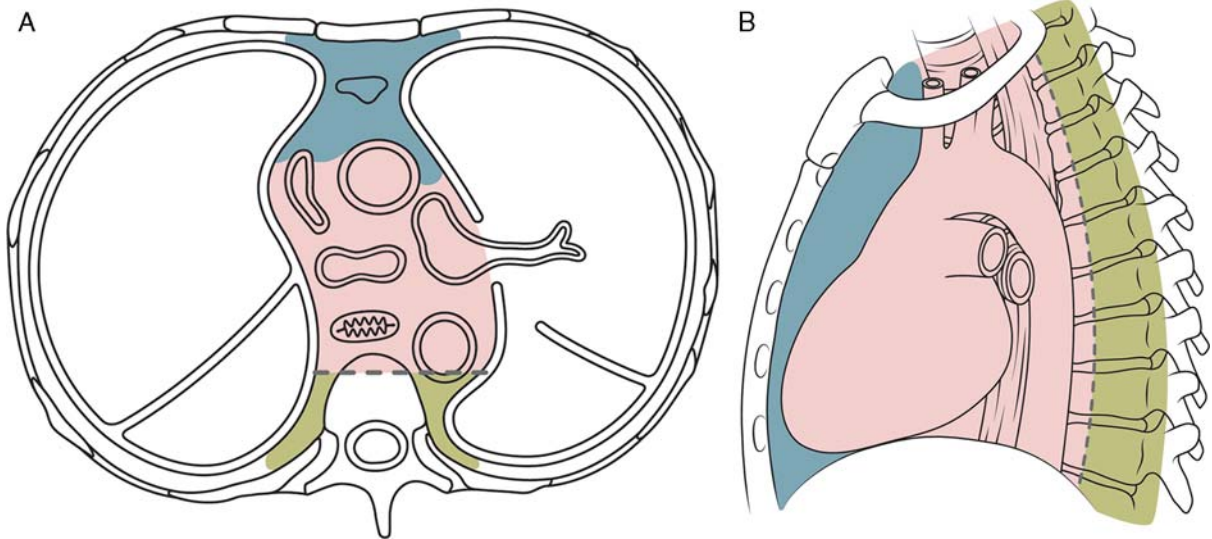


FIGURE 1. Schematic illustration for the new definition of mediastinal compartments based on the CT images in axial (A) and sagittal planes (B). Prevascular compartment: blue. Visceral compartment: pink. Paravertebral compartment: green. Visceral-paravertebral compartment boundary: dashed line.

represents the anterior margin, whereas the anterior aspect of the pericardium represents the posterior margin. As the pericardium extends along the anterior margins of the ascending aorta, the aortic arch lateral rim, the superior vena cava anterior margin, and along the superior and inferior pulmonary veins, these structures are not included in the prevascular compartment. The differential diagnosis for prevascular compartment masses includes lymphoma, metastatic disease, thymic abnormalities and thymic variants, germ cell neoplasms, and intrathoracic goiter (Table 1).⁴ Each of these entities along with diseases primarily affecting the visceral and paravertebral compartments will be discussed in detail below.

Like the prevascular compartment, the visceral compartment is bounded inferiorly by the diaphragm and superiorly by the thoracic inlet. The posterior boundary of the prevascular compartment forms its anterior border, whereas the posterior border is defined by a series of vertical lines connecting points on each vertebral body 1 cm posterior to the vertebral body anterior cortex.⁴ Major

prevascular contents include vascular structures, for example, heart, aorta, intrapericardial pulmonary arteries, thoracic duct, and superior vena cava, and nonvascular structures, for example, esophagus, trachea, and lymph nodes. Visceral compartment abnormalities include malignant and reactive lymphadenopathy, tracheal and esophageal lesions, foregut duplication cysts, and lesions of the pericardium, heart, and great vessels (Table 1).

The paravertebral compartment is delimited superiorly by the thoracic inlet, inferiorly by the diaphragms, anteriorly by the posterior border of the visceral compartment, and posterolaterally by a vertical line along the posterior chest wall margins adjacent to the lateral margins of the thoracic transverse processes. The paravertebral compartment major contents include the paravertebral soft tissues.⁴ As such the primary abnormalities in this compartment include neurogenic tumors (Table 1). Traumatic lesions and infection may also affect soft tissues in this compartment.

With consideration for each compartment and the general differential diagnosis based on compartmental location, it is imperative to have an understanding of the relative strengths and weaknesses for individual imaging modalities, practical imaging algorithms, and a detailed understanding of the individual imaging findings and management issues for each mediastinal mass. This article attempts to address these issues and to increase the readers' understanding of the imaging evaluation of mediastinal masses detected in pediatric and adult patients.

CURRENT IMAGING MODALITIES AND TECHNIQUES

To develop an accurate and cost-effective imaging plan, there are 4 primary goals when imaging mediastinal masses: (1) identification and accurate compartmental localization; (2) detailed mass description; (3) provision of an accurate and succinct differential diagnosis; (4) recommendation of a cost-effective imaging and patient management plan. Currently, available modalities for mediastinal mass evaluation include: CR, ultrasound (US),

TABLE 1. Differential Diagnostic Possibilities Based on The New CT-Based Mediastinal Department Classifications

Compartment	Differential Diagnosis
Prevascular	Thymic lesions/masses Germ cell neoplasms Lymphoma Intrathoracic goiter
Visceral	Metastatic lymphadenopathy Lymphoma Metastatic lymphadenopathy Foregut duplication cysts Tracheal lesions Esophageal masses Aortic aneurysms Cardiac masses
Paravertebral	Pericardial masses/cysts Benign and malignant peripheral nerve tumors Sympathetic ganglia tumors Lateral thoracic meningocele Extramedullary hematopoiesis

MDCT, magnetic resonance imaging (MRI), and nuclear medicine studies.

CR

In nearly all cases, CR represents the first modality in imaging mediastinal masses and is advantageous because of its relative low cost, widespread availability, and ease of acquisition. There are disadvantages, particularly in the pediatric population, relating to the use of ionizing radiation and overall poor performance in comparison with other imaging studies. In comparison with MRI and MDCT, CRs have decreased sensitivity for detecting small mediastinal masses. Moreover, rarely can a definitive diagnosis be made solely on CR, necessitating additional cross-sectional imaging. The exact technique used is dependent on patient age, but obtaining both frontal and lateral radiographs is preferable. In the very young or the very sick, a lateral radiograph may not be feasible, and a supine frontal radiograph must suffice. Occasionally, a cross-table lateral can be performed to more accurately localize the lesion if a true lateral is unobtainable.

US

Because of suboptimal acoustic windows, US has a limited role in adults and children above 5 years of age, which represents its major disadvantage. However, in young children its usefulness increases and is particularly advantageous in differentiating a prominent but otherwise normal thymus from a true mediastinal mass. Other advantages include its lack of ionizing radiation, portability, widespread availability, and capability for real-time scanning evaluation. Typical technique includes imaging through the suprasternal, parasternal, sternal, subxiphoid, and intercostal approaches with the patient lying supine. Prone and decubitus positions may also be needed depending on the mediastinal compartment involved.⁵ Transducer selection is based on patient age and size. A 5 to 10 MHz linear-array transducer is used in infants and neonates. In older children and adults a 2 to 4 or 4 to 7 MHz linear-array or sector transducer may be needed.⁵ Images are acquired in at least 2, if not 3, orthogonal planes. Doppler may be added to define internal vascularity.

CT

Despite the increased utilization of US in pediatrics, CT, specifically MDCT, continues to have a prominent role in the imaging of pediatric and adult mediastinal masses. Advantages are plentiful and include widespread availability, imaging acquisition speed, which has significantly decreased the need for sedation in young children, and its high spatial resolution. MDCT has been specifically shown to have a high accuracy for characterizing the size, location, and adjacent organ involvement in the evaluation of mediastinal masses^{1,6} as well as affecting clinical management in 65% of cases and adding additional diagnostic information in 82%.^{1,6,7} The primary disadvantage of CT lies in its relatively high radiation dose, although this particular disadvantage is subject to much current research and technical innovation.⁸

MRI

Given its superior tissue-contrast resolution and lack of ionizing radiation, MRI has been increasingly utilized for mediastinal mass evaluation in children and adults. Its historical disadvantages have progressively decreased with significant research and clinical interest in providing

superior contrast resolution and spatial resolution near that of CT while decreasing the need for sedation through novel ultrafast sequences. MRI provides both physiological and anatomic data, unlike other imaging modalities. Furthermore, MRI is able to differentiate internal mass constituents, particularly cystic from solid components, which CT struggles to define.

Specific MRI protocols vary depending on institutional preferences and equipment availability, but some general principles and sequences are worth consideration. If available, an 8-channel or greater cardiac coil is recommended. Useful sequences include: coronal fast-recovery fast spin-echo (FRFSE) T2 with fat saturation; axial FRFSE T2 with fat saturation; axial T1 or double inversion-recovery sequence; coronal gadolinium-enhanced 3-dimensional MR angiography spoiled gradient-recalled echo sequence; and postgadolinium, fat-saturated axial and coronal T1 sequences. Breath-holding or respiratory triggering is recommended for the FRFSE sequence to reduce motion artifact. Electrocardiography gating and a breath-hold are needed to optimize the double inversion-recovery sequence.

Nuclear Medicine Studies

Available nuclear medicine studies for mediastinal mass evaluation primarily include positron emission tomography (PET) often coregistered with CT (PET/CT) and metaiodobenzylguanidine (MIBG) imaging. Historically, gallium-67 imaging represented an additional nuclear medicine test used in mediastinal lymphoma but is rarely utilized today.

Although PET/CT is not currently the first-line modality for the evaluation of mediastinal masses, it has become a near first-line modality for tumor staging, treatment response assessment, and postcompletion therapy assessment in lymphoma.^{1,9-14} In comparison with other imaging techniques, PET is superior for differentiating scar and nonviable residual tissue from viable tumor, detecting tumor foci within normal-appearing lymph nodes, and extranodal sites of disease.¹ Given these advantages, PET may also be useful in other mediastinal tumors, particularly malignant and metastatic masses.

Typical protocols include a 6-hour fast before 2-fluoro-2-deoxy (18 fluorine)-d-glucose (18FDG) injection. Oral and intravenous contrast may be administered depending on institutional preference. Often the PET data set is coregistered with CT with the technique varying from low-dose, non-diagnostic scans to full diagnostic quality images.

MIBG represents a guanethidine analog, similar to norepinephrine, radiolabeled with I-123. Once injected, chromaffin cells within abnormal sympathetic adrenergic tissue take up MIBG allowing it to serve in the imaging evaluation of posterior mediastinal neurogenic tumors. A detection rate of 90% to 95% has been found with neuroblastoma.¹⁵ After administration, whole-body planar images are obtained at 24 to 48 hours.

PRACTICAL IMAGING ALGORITHM

The first step in accurate description of mediastinal masses is to correctly characterize the lesion as mediastinal in origin. Although this statement seems to be intuitive, very large mediastinal masses can extend into and fill 1 or both hemithoraces, mimicking a lung parenchymal or pleural mass. On the same note, large lung parenchymal

masses can extend into the mediastinum simulating a mediastinal lesion. As such, 2 straightforward approaches have been proposed to help in accurately localizing mediastinal masses.

The simplest method, termed the “center method,” begins with localizing the center of the lesion on the axial image where the largest diameter of the lesion is demonstrable.⁴ The center represents the theoretical beginning of the lesion and has been shown to accurately classify masses to a specific mediastinal compartment in a study of 445 mediastinal masses.³ If the exact compartment of origin remains in question after scrutiny of the axial images, coronal and sagittal series may be of value. The second method is called the “structure displacement tool.”⁴ In this method, the compartment of origin is identified by the shifting of structures from other mediastinal compartments as well as the direction of displacement.⁴ For example, large paravertebral compartment masses displacing the heart and trachea anteriorly and to the contralateral side. In their updated description of mediastinal compartments, the ITMIG recommended the utilization of both of these tools to localize mediastinal masses.⁴

Once the compartment of origin is determined, the mass should be further subcategorized into its structural constituents. In other words, on the basis of its imaging characteristics such as Hounsfield unit (HU) values and amount and distribution of enhancement, it is determined whether the mass is cystic or solid, whether there are fatty or calcific components, and whether the mass is intimately associated with certain key structural features such as extension along subcostal nerve roots. By accurate lesional and compartmental characterization, a defined differential diagnosis can be proposed and further refined in select cases to a specific diagnosis.

SPECTRUM OF IMAGING FINDINGS

Prevascular Compartment Masses

Soft Tissue Masses

Thymus: The thymus is located in the prevascular compartment and is an encapsulated, bilobed, immune system organ. It primarily functions as a site for T-lymphocyte maturation. Its imaging appearance varies across the age spectrum (Fig. 2), which can lead the unaware radiologist to errantly mistake a normal thymus for a mediastinal mass, especially in young children in whom the thymus may have bulging/convex lateral margins. Thus, it is imperative for radiologists to be aware of the shape changes the thymus undergoes during childhood and early adulthood. These are best appreciated and most often encountered on CR.

On CR, the thymus appears as a quadrilateral prevascular soft tissue density with outward convex borders from infancy until about 5 years of age. Around this time, the thymus develops straight margins, taking on a triangular configuration. The margins progressively become concave after age 15 until the thymus completely or nearly completely involutes in adulthood.² If the radiologist is still in doubt after the initial CR and the patient is less than 5 years of age, US is generally the next best test for evaluation.

On US, the thymus appears as a smoothly margined, well-defined organ of uniform echogenicity, which molds to the adjacent structures and deforms with vascular and cardiac pulsations. The overall echogenicity closely resembles that of the liver with multiple hyperechoic septations scattered throughout the gland.

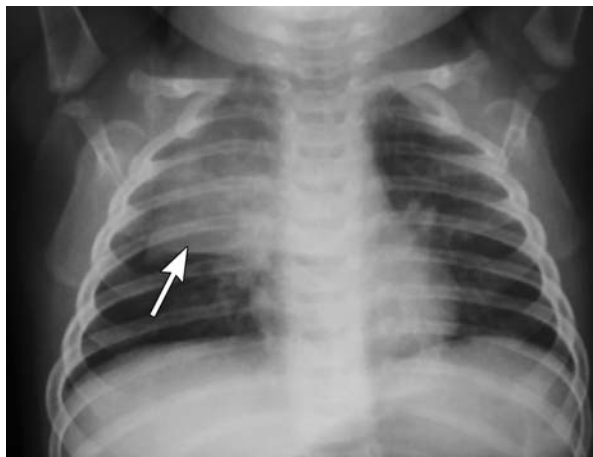


FIGURE 2. Frontal CR of a young child demonstrates the classic “thymic sail sign” (arrow), a normal thymic variant appearance and not to be mistaken for a mediastinal mass or pneumomediastinum. (Image provided courtesy of Ramon Sanchez, MD, Department of Radiology, University of Michigan Medical Center, C.S Mott Children’s Hospital.)

CT and MRI are rarely required for normal thymus evaluation, but the thymus is frequently demonstrated on these modalities when performed for alternative indications. Similar to US, the CT and MRI appearance of the thymus is that of a smoothly margined, homogenous gland conforming to the adjacent mediastinal structures (Fig. 3). No compression or displacement of the surrounding anatomy should be present. Thymic CT attenuation and MRI signal characteristics change over time to reflect gradual fatty glandular replacement.¹⁶ Although these findings often help differentiate normal thymus from other anterior mediastinal abnormalities, 2 specific entities, that is, thymic variants and thymic hyperplasia, may cause confusion even in the experienced radiologist and warrant further discussion.

Notable thymic variants that may be mistaken for a pathologic mediastinal mass are suprasternal and retrocaval extension of the thymus. Of these 2, suprasternal extension is much more common and can be seen in up to 2/3 of infants and young children.¹⁷ Here, the thymus extends superior to the manubrium and into the anterior-inferior neck (Fig. 3). In a retrospective review of 200 patients, Costa et al¹⁷ proposed several criteria for differentiating cervical extension from a pathologic mass on MRI, which include its appearance as a well-defined lobe of soft tissue, which is isointense to the main thymus, extending anterior to the trachea and great vessels in the base of the neck, and is in direct continuity with the main thymus. Although this may be appreciated on axial images, sagittal and/or coronal CT or MRI images are most helpful in showing the superior extension and direct continuity with the main thymus (Fig. 3).

Retrocaval extension is rarer and appears as posterior thymic extension between the great vessels and superior vena cava. On CR, retrocaval extension may be confused for right upper lobe collapse or paratracheal lymphadenopathy. On CT or MRI, retrocaval thymic extension may be differentiated from a pathologic mediastinal mass by observing its continuity with normal thymic tissue and its homogenous attenuation or signal intensity, which matches that of the anteriorly positioned normal thymus.²

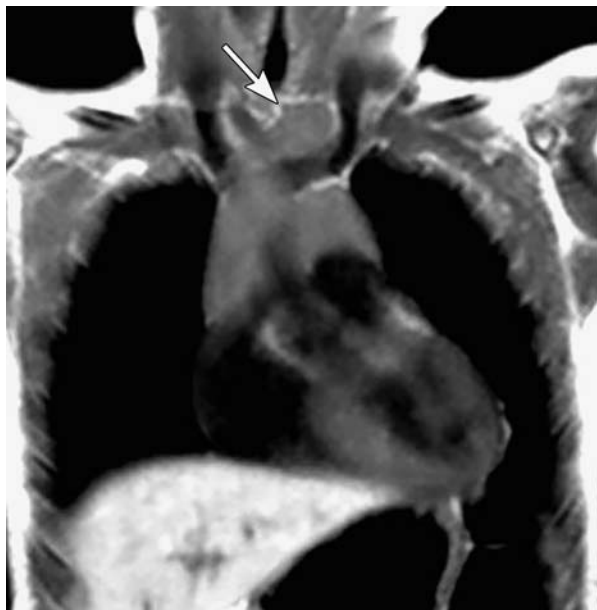


FIGURE 3. Normal variant cervical extension of the thymus in a 4-year-old boy. Coronal turbo spin-echo T1-weighted image showing extension of a normal thymus (arrow) into the lower neck. Note the absence of compression on adjacent vascular structure and homogenous appearance of the normal thymus. These findings help in differentiating this thymic variant from a true mediastinal or neck base mass.

Similarly, it may be difficult to distinguish thymic hyperplasia from other prevascular mediastinal abnormalities. Thymic hyperplasia occurs in 2 forms: lymphoid hyperplasia and true thymic hyperplasia. Of these 2, lymphoid or follicular hyperplasia is more commonly seen clinically and occurs in up to 2/3 of myasthenia gravis patients.¹⁸ Most commonly, the thymus is normal in size and shape. However, occasionally, lymphoid and follicular hyperplasia may present as diffuse thymic enlargement (Fig. 4A) or as a focal thymic mass (Fig. 4B). Nevertheless, to our knowledge no imaging findings have been described to date to differentiate between lymphoid and follicular thymic hyperplasia.

True thymic hyperplasia results from increase in both the size and shape of the thymus while preserving thymic architecture, most commonly after atrophy resulting from medications, severe illness, or surgery. In 90% of cases, the thymus will atrophy after chemotherapy.² Upon recovery, the thymus increases in volume, returning to its original size or possibly exceeding its baseline value by up to 50%.¹⁹ Recently, CT attenuation values have been shown to be significantly higher in lymphoid hyperplasia compared with true thymic hyperplasia with 41 HU being deemed an optimal threshold for differentiation between the 2.²⁰ However by CT alone, it may be difficult to distinguish thymic hyperplasia from tumor recurrence, particularly in the setting of thymic involvement by lymphoma. If on CT a prevascular mass has a bipyramidal morphology with the presence of gross intercalated fat, these findings are pathognomonic for thymic hyperplasia.²¹ Nevertheless, these findings are not always present. In such cases, MRI or PET imaging can be beneficial.

On MRI, in-phase and out-of-phase gradient-echo imaging has been shown to accurately differentiate normal

thymus and thymic hyperplasia from thymic neoplasms.^{16,22} In a prospective study by Inaoka et al,²² the authors found uniform suppression of normal thymus and thymic hyperplasia on out-of-phase imaging due to interspersed microscopic fat, whereas thymic neoplasms uniformly did not suppress. Thus, MRI shows a unique ability to confirm the diagnosis of thymic hyperplasia without imparting radiation. Nevertheless, the diagnostic conundrum of thymic hyperplasia versus recurrent neoplasms often first arises on follow-up/off-therapy PET/CT. Here a standardized uptake value of <3.4 suggests thymic hyperplasia.⁹

Thymoma: In contrast to children, in whom thymomas are rare and represent only 1% to 2% of pediatric prevascular mediastinal masses, thymomas are much more common in adults, comprising 20% of adult mediastinal neoplasms.^{2,19} Pathologically, thymomas are a thymic epithelial neoplasm containing a varied amount of lymphocytes, with 40% of patients presenting with paraneoplastic symptoms, most commonly myasthenia gravis.² Historically, thymomas are categorized as invasive or noninvasive with the divisions predicated on tumor extension beyond the surrounding fibrous capsule. However, this demarcation is often only demonstrated during pathologic analysis. As such, imaging is limited in its ability to differentiate between the 2, and usage of the terms “invasive” and “noninvasive” thymoma is discouraged in image reporting. As staging is primarily surgical/pathologic, imaging helps to guide surgical planning providing a “presurgical” staging, which has been shown to closely correlate with surgical/pathologic staging.²³ Thus, imaging findings such as macroscopic invasion of adjacent structures, pleural and pericardial metastasis, and distant metastatic disease should be sought for and described.^{24–26}

On CR, thymomas generally appear as an oval, prevascular mass with smooth margins and obliteration of the retrosternal clear space. Occasionally, the fibrous capsule may have a thin rim of calcification.² As the lesion increases in size and extends through the capsular margins, the borders may become irregular, the interface with the adjacent lung may be indistinct, and pleural nodules may be seen. Once identified, CT or MRI may be performed.² On CT, thymomas appear as well-defined, rounded or lobulated soft tissue density masses with associated mild enhancement (Fig. 5). Similar to CR, as the masses invade adjacent mediastinal fat and normal mediastinal structures, CT findings include irregular borders, extension into the adjacent pleura, the diaphragm or the chest wall, and pleural nodules. Thirty percent of thymomas will have necrosis and internal cystic foci.² If an MRI is performed, thymomas appear similar morphologically to that on CT and are uniformly or heterogeneously hyperintense on T2 with mild associated enhancement.² Dynamic MRI imaging, for example, the MRI “sniff test,” may be used to provide a functional assessment of diaphragmatic motion and phrenic nerve involvement by the mass. In such cases, the tumor would be considered to be stage III with neoadjuvant chemotherapy likely administered before surgery.^{24,27}

Thymic Carcinoid: Thymic carcinoid is a rare, highly aggressive tumor arising from neural crest cells within the thymus and occurs across the age spectrum with a median age of 43 years.^{28,29} In children, nearly all patients present with Cushing syndrome. In contrast, only 25% to 40% of adult patients present with endocrine disorders.³⁰ Most thymic carcinoids occur in male patients with a 3:1 male to

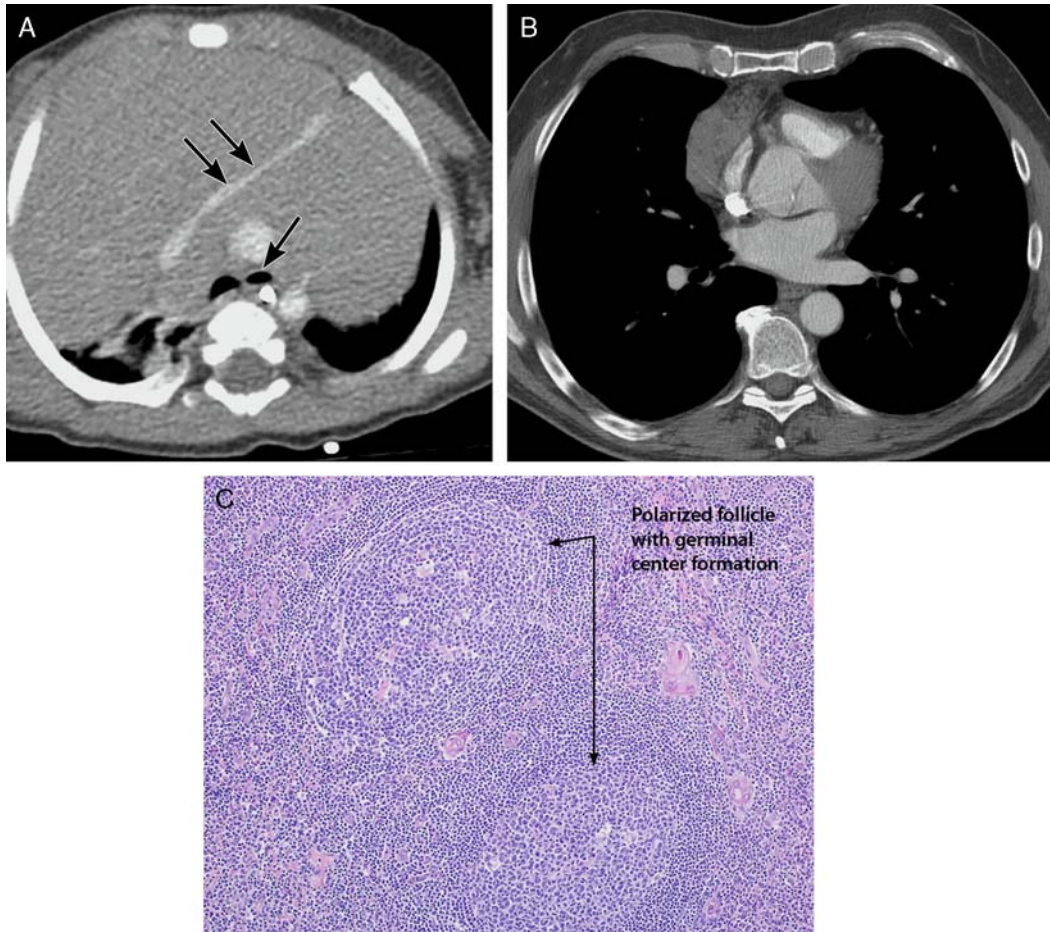


FIGURE 4. Thymic lymphoid hyperplasia in a 7-month-old girl with Beckwith-Wiedemann syndrome presenting with cough. A, Axial contrast-enhanced chest CT demonstrates marked enlargement of the thymus with compression on left brachiocephalic vein (double arrow) and narrowing of the airways (arrow). B, Thymic follicular hyperplasia in a 60-year-old man with prostate cancer status post radical prostatectomy. During evaluation for increasing prostate-specific antigen level, a prevascular mediastinal mass was noted on chest CT. Biopsy showed thymic hyperplasia. C, Histologic slide corresponding with the axial CT image in (A) demonstrates hyperplastic polarized lymphoid follicles with germinal centers. No evidence of lymphoma or malignancy is seen.

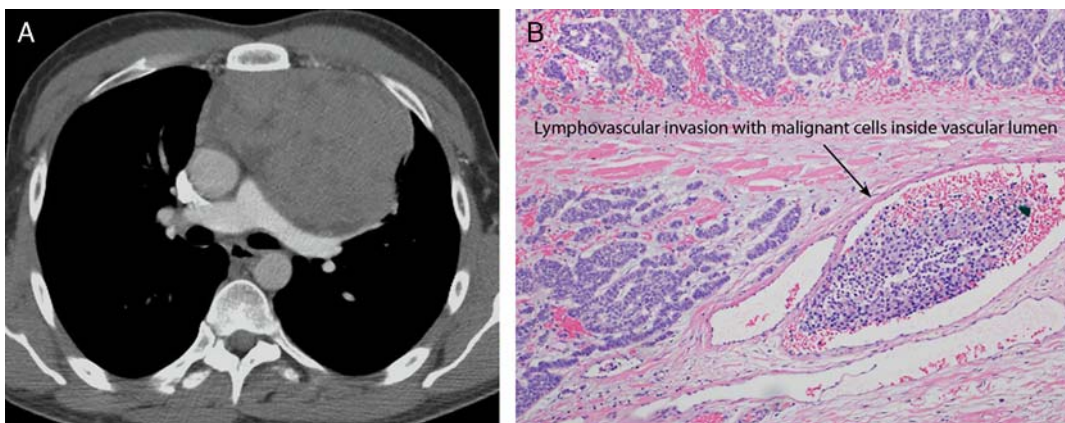


FIGURE 6. Thymic carcinoma in a 31-year-old man with multiple endocrine neoplasia. A, Axial contrast-enhanced chest CT at the level of the pulmonary artery bifurcation demonstrates a large heterogeneous mass within the prevascular compartment compressing and displacing the pulmonary arteries and left main stem bronchus. These findings are nonspecific, and other mediastinal lesions may have this appearance necessitating pathologic confirmation. B, Lymphovascular invasion as evidence of malignant behavior in this histologically proven thymic carcinoma.

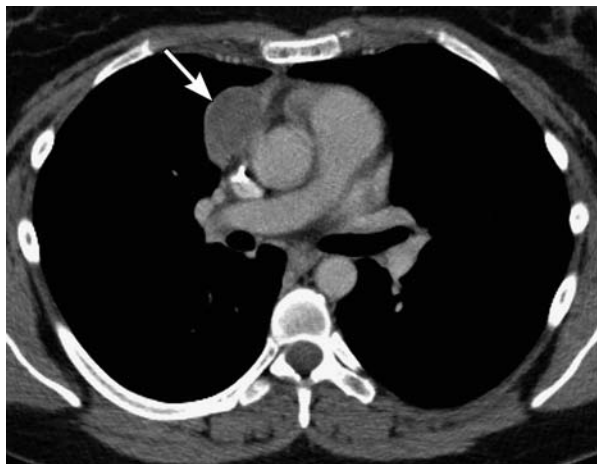


FIGURE 5. 38-year-old woman with a thymoma. Axial contrast-enhanced chest CT image demonstrates a homogenous, well-defined, mass (arrow) within the prevascular mediastinal compartment, which is lower attenuation than the adjacent enhanced aorta. CT findings of a well-circumscribed, oval or round, off-midline prevascular, soft tissue mass favors thymoma over other prevascular mediastinal lesions.

female ratio.²⁹ Thymic carcinoids can occur in isolation or in association with multiple endocrine neoplasia, specifically type I.^{20,31–34}

The imaging appearance of thymic carcinoid is nonspecific, and it may be difficult to differentiate them from other invasive thymic neoplasms. They are often large at presentation with complete obliteration of the retrosternal clear space on CR. On CT or MRI, thymic carcinoids demonstrate a heterogeneous enhancement pattern with areas of necrosis and invasion of adjacent mediastinal structures.²⁹ On PET imaging, they are often FDG avid.³⁵

Thymic Carcinoma: Thymic carcinomas rarely occur in the pediatric population and typically arise in the fifth and sixth decades of life. They are aggressive epithelial neoplasms with almost all patients symptomatic at presentation.² Given their adult age predilection, although still rarely occurring in children, both pediatric and adult imagers must be aware of their imaging features.

On CR, thymic carcinomas most often appear as irregular, large anterior mediastinal masses obliterating the retrosternal clear space. Internal dystrophic calcification may be seen on CRs but are better appreciated on CT. Thymic carcinomas on CT typically demonstrate irregular or lobulated margins with focal areas of decreased attenuation representing changes from prior hemorrhage, necrosis, or cyst formation (Fig. 6). Invasion of the adjacent normal thoracic structures, such as the great vessels and bony thorax, as well as pericardial and pleural effusions may be seen, although these are not always present.³⁶ The MRI appearance of thymic carcinoma is similar to that of CT with heterogeneous signal intensity within a large, irregular, prevascular mass. On both CT and MRI, thymic hyperplasia may be difficult to differentiate from high-risk thymoma. However, heterogeneous contrast enhancement, cystic or necrotic components, great vessel invasion, and lymphadenopathy are significantly more likely to be present in thymic carcinoma compared with thymoma.³⁷ Compared with CT, MRI has been shown to be superior for depicting

intratumoral hemorrhage.³⁷ In addition, diffusion-weighted MRI imaging can differentiate low-risk thymoma from high-risk thymoma and thymic carcinoma by the quantitative analysis of apparent diffusion coefficient (ADC) values. In a prospective study of 30 patients, Razek and colleagues found a statistically significant difference in ADC values, with low-risk thymoma having a higher ADC value compared with high-risk thymoma and thymic carcinoma.³⁸ These findings led the authors to conclude that ADC values are a reproducible and reliable imaging parameter when characterizing thymic epithelial neoplasms and should be routinely performed when assessing these neoplasms.³⁸

Thyroid: Intrathoracic thyroid goiter affects approximately 5% of patients with thyroid disease and represents 10% of mediastinal masses. Seventy-five percent to 90% of cases involve the prevascular compartment and 10% to 25% occur within the paravertebral compartment.^{39–42} Intrathoracic goiter can be classified as primary or secondary, with the large majority representing secondary intrathoracic goiter, arising from the thyroid tissue within the neck and extending into the mediastinum.³⁹ Rarely, thyroid malignancy may invade into the prevascular compartment by direct extension.

On CR, prevascular thyroid goiter appears as a soft tissue mass within the base of the neck and prevascular mediastinal compartment, filling the retrosternal clear space, and displacing the trachea and great vessels with tracheal deviation seen in up to 37% of thyroid surgery patients on preoperative CR.⁴³ Despite this fact, Hong et al⁴³ found no correlation between tracheal deviation and increased difficulty with intubation, leading the authors to conclude that routine CR before thyroid surgery is not warranted. In contrast to tracheal deviation, tracheal compression with variable degrees of obstruction is highly associated with substernal goiter, found in up to approximately 97% of patients. Compression may be less readily apparent on CR as compared with CT and MRI, and advanced cross-sectional imaging may be warranted before surgery, particularly in patients presenting with substernal goiter and dyspnea. These findings are helpful in alerting the anesthesia team before attempted intubation, as tracheal compression with an inability to ventilate is a feared complication in substernal goiter patients undergoing anesthesia. On nonenhanced CT, goiters measure >100 in HU due to the thyroid concentration of iodine and have intense and prolonged enhancement after contrast administration. Frequently, calcifications are seen. MRI exquisitely demonstrates goiter extension from the thyroid as a prevascular, T2 hyperintense mass and has been shown to be useful for the evaluation of thyroid goiter in both the prenatal and postnatal child.⁴⁴

In contrast, intrathoracic thyroid malignancy has a variable appearance on CT and MRI with borders ranging from well-defined to ill-defined. Enhancement is heterogeneous and adjacent invasion of normal mediastinal structures may be seen.⁴¹

Lymphoma: Lymphoma is the third most common pediatric malignancy and is the most common pediatric prevascular mass.^{1,2} Conversely, lymphoma represents only 2% to 10% of prevascular mediastinal masses in patients greater than 40 years old.⁴⁵ Lymphoma has been traditionally divided into Hodgkin and non-Hodgkin lymphoma (NHL), with Hodgkin characterized histologically by Reed-Sternberg cells and NHL by T-lymphocyte or B-lymphocyte clonal proliferation. Hodgkin lymphoma more



FIGURE 7. T-lymphoblastic lymphoma in a 9-year-old boy presenting with cough. Axial CT image of the chest using intravenous contrast shows a prevascular mediastinal mass with compression on the left brachiocephalic vein and significant narrowing of the airways (arrow). Given the patient's age, lymphoma would be the primary consideration for these CT findings.

commonly affects the thorax, but 50% of NHL cases have thoracic involvement.²

The CR appearance of lymphoma is typically that of a large prevascular mass (Fig. 7).¹ After CR, CT or MRI may be utilized for diagnostic confirmation and disease staging. On both modalities, lymphoma appears as either separate or confluent areas of lymphadenopathy or as a single large, lobular, often heterogenous mass, which displaces adjacent normal structures and may invade the thymus. In comparison with thymoma, lobulations, nodularity, and mid-line location on CT are significantly more likely in lymphoma.²¹ Pleural effusions, pulmonary nodules, and chest wall involvement may be seen. Calcifications can occur after treatment, but are extremely rare in the pre-treatment setting.¹

Over the last decade, PET or combined PET/CT has supplanted traditional anatomic imaging for lymphoma staging and treatment response, with PET being more sensitive than MRI and CT alone for evaluating tumor presence within normal-sized lymph nodes. Nevertheless, there is significant interest in reducing or eliminating radiation-yielding imaging modalities for lymphoma evaluation and staging, particularly given its pediatric age propensity. Recent advanced MRI techniques evaluated for this purpose include diffusion-weighted imaging (DWI) and dynamic MRI. In comparison with PET, Mayerhoefer et al⁴⁶ found DWI to be only slightly inferior to PET/CT in the pretherapeutic staging and regional assessment in FDG-avid lymphoma. However, the authors demonstrated DWI to be superior to PET in tumors with variable FDG avidity. Similarly, Punwani et al⁴⁷ found DWI to compliment PET in the assessment of treatment response, with tumors with adequate treatment response showing a significantly lower median pretreatment ADC than those with inadequate treatment response. Such findings suggest that MRI has the potential to replace CT in PET imaging with PET/MRI, although this modality is not currently widely available. Lastly, dynamic MRI has been shown to be useful in

differentiating lymphoma and thymoma, with lymphoma having a significantly longer time to peak enhancement.⁴⁸ These findings suggest that MRI will have an increased role in imaging of mediastinal lymphoma, with the potential to reduce, or possibly eliminate the need for other radiation-yielding imaging.

Fatty Masses

Lipoma: Similar to lipomas arising in other areas of the body, prevascular lipomas are well-encapsulated fatty masses with an identical composition to subcutaneous fat. Generally, they are asymptomatic due to the mass's pliability, incidentally detected on imaging performed for an alternative reason.

On CR, lipomas appear as a well-defined mass with convex borders. The mass may be radiolucent relative to the adjacent soft tissues. The fatty composition of these lesions are well demonstrated on both CT and MRI, with CT demonstrating a smoothly margined mass of fatty attenuation. If MRI is performed, the mass is hyperintense on T1-weighted images becoming hypointense with fat saturation on T1-weighted and T2-weighted images. Post-gadolinium images demonstrate no internal enhancement.

Liposarcoma: Liposarcoma is the most common malignant mediastinal mesenchymal tumor and most commonly arises in the prevascular mediastinal compartment.⁴⁹ Patients may be asymptomatic with a mass found incidentally on imaging obtained for an alternative indication. If symptomatic, patients may present with tachypnea, superior vena cava syndrome, chest pain, and weight loss.

On imaging, mediastinal liposarcomas have similar imaging characteristics as those found in liposarcomas elsewhere in the body and can range from predominantly fatty prevascular mediastinal masses to a solid mass lesion with little to no macroscopic fat evident.^{50,51} Given the fatty components, it may be difficult to distinguish liposarcomas from lipomas, thymolipomas, and mediastinal germ cell tumors. However, like elsewhere in the body, liposarcoma should be the primary consideration in large prevascular mediastinal masses containing predominantly enhancing soft tissue components with little interspersed fatty areas.

Germ Cell Tumors: Prevascular mediastinal germ cell tumors account for 6% to 18% of pediatric mediastinal masses and <5% of adult prevascular mediastinal masses.⁴⁵ They are typically located within or near the thymus and result from halted migration of primitive germ cells to the gonads. Most are benign (mature) teratomas. However, 14% are malignant teratomas (immature), with nonteratomatous germ cell tumors being rare.^{1,2,52-54}

Mature and immature teratomas appear as large, well-circumscribed masses on CR. Dystrophic calcifications may occur in 25% and may be helpful in suggesting the appropriate diagnosis on radiographs alone.² Generally, CT or MRI is utilized after CR and demonstrate a complex solid and cystic mass (Figs. 8, 9). Hallmarks of both benign and malignant teratomas include fluid, fat, and calcific components.^{1,2,55-58} Demonstration of enhancing soft tissue components serves as a suggestive, but not definitive, differentiator between benign and malignant lesions, as malignant teratomas are more likely to have enhancing soft tissue components (Fig. 9).² An additional feature that helps to differentiate between teratoma subtypes is invasion of adjacent normal mediastinal structures, a feature suggestive of malignancy.² Nevertheless, it is not always possible to differentiate mature from immature teratomas by

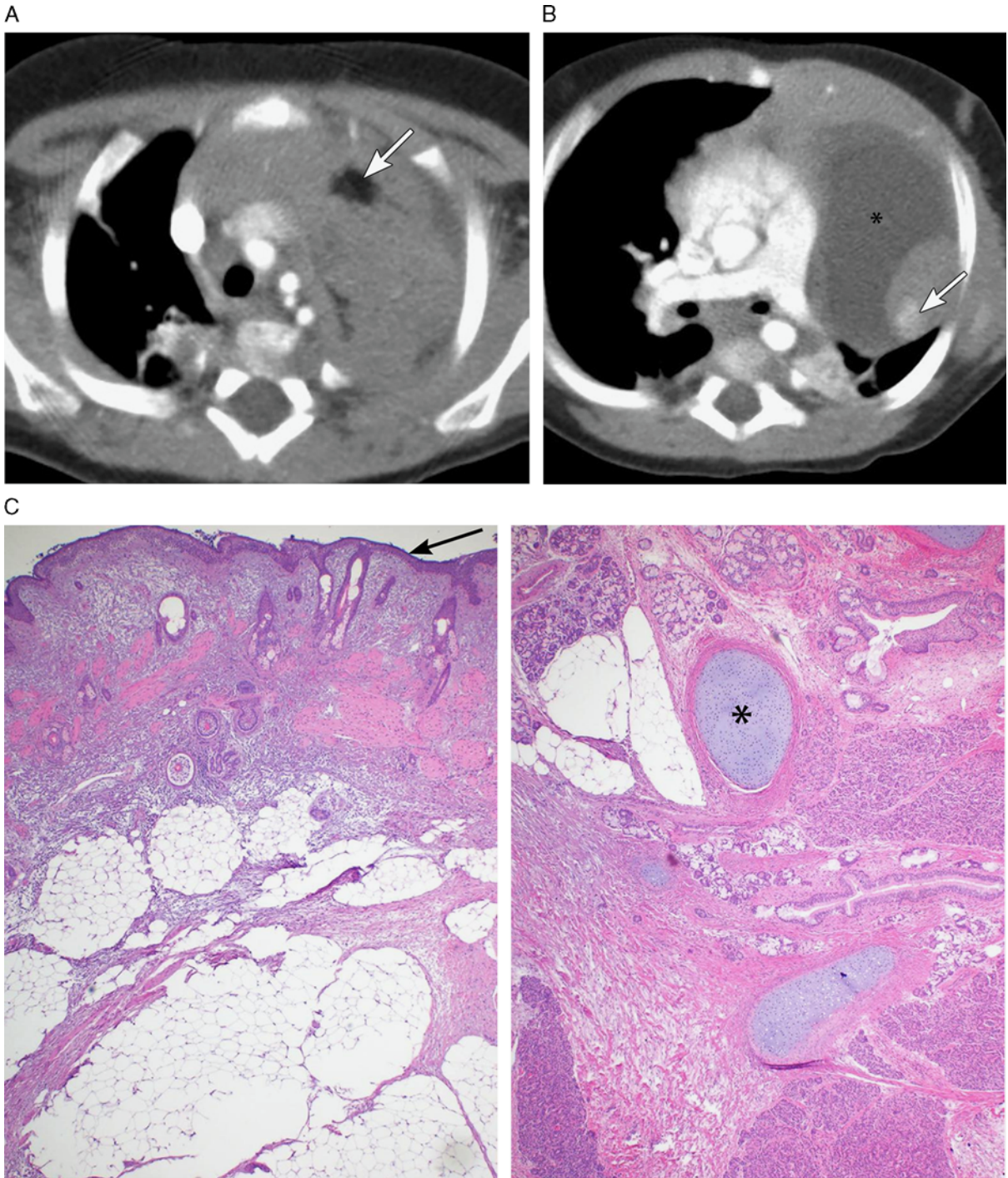


FIGURE 8. 4-month-old boy with a 5-day history of cough. A and B, Axial CT images with intravenous contrast shows a prevascular compartment mass with areas of fat (arrow in A), calcification (arrow in B), and fluid attenuation (* in B) suggestive of a teratoma. C, Mature germ cell neoplasm with structures derived from all 3 embryonic layers: skin (arrow), ectoderm; cartilage (*), mesoderm; pancreas and intestinal structures, endoderm. Teratomas may be difficult or impossible to distinguish from other prevascular mediastinal masses in the absence of macroscopic fat or calcifications. However, in (B), all 3 constituents of a teratoma are readily demonstrated allowing for the confident diagnosis of a mediastinal germ cell neoplasm.

imaging alone, with laboratory analysis being crucial in such settings. If the teratoma ruptures and the intrapulmonary bronchus is affected, obstructive pneumonitis may develop.

Nonteratomatous germ cell tumors are divided into seminoma and nonseminomatous germ cell tumors. At imaging, seminomas often appear as large, lobulated prevascular mediastinal masses, which are homogenous on cross-sectional

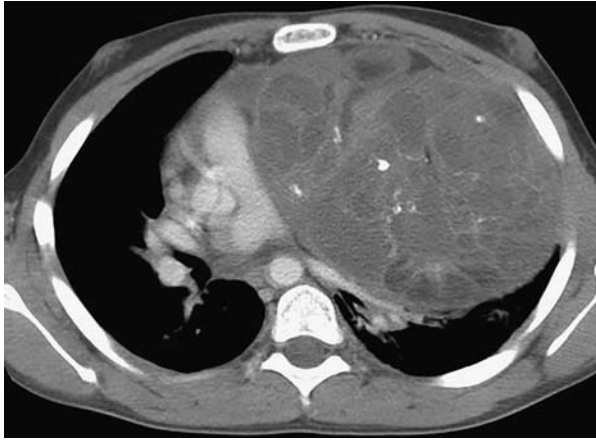


FIGURE 9. 13-year-old girl with increasing fatigue and shortness of breath. Axial chest image with intravenous contrast shows a large heterogenous mass with soft tissue, fat, fluid, and calcification in a biopsy-proven immature teratoma. Note compression of the main pulmonary artery.

imaging and rarely invade adjacent normal mediastinal structures.⁵⁹ In advanced stages, lymph node and bone metastasis can be seen. In contrast, nonseminomatous germ cell tumors are most often heterogenous on cross-sectional imaging with foci of necrosis and hemorrhage. Invasion of adjacent mediastinal structures is more common with distant site and regional node metastasis in advanced disease. Regardless, both seminoma and nonseminomatous germ cell tumors may be difficult to distinguish from other malignant anterior mediastinal masses with a reported diagnostic accuracy of 35% by CT alone, 27% by MRI alone, and 31% by CT and MRI in combination.⁵⁹ Thus, imaging alone may not provide a definitive diagnosis, although imaging in concert with elevated tumor markers, that is, α -fetoprotein and/or human chorionic gonadotropin, may point to the ultimate diagnosis.⁶⁰

Cystic Masses

Thymic Cyst: Thymic cysts may be congenital or acquired and are a rare cystic, fluid-filled mass in the prevascular compartment. Although thymic cysts are generally found in the infrahyoid neck, they may be found anywhere from the pyriform sinus to the prevascular mediastinum. When congenital they most commonly originate from the thymopharyngeal duct remnant and are unilocular with barely perceptible walls on imaging.¹⁶ In contrast, acquired thymic cysts occur after inflammation, particularly in association with human immunodeficiency virus, and are often multilocular.^{16,61}

On CR, thymic cysts are often occult, being obscured by the normal thymus. However, with CT or MRI, they become much more conspicuous. On both, thymic cysts most often appear as well-defined, smooth-walled, non-enhancing cystic lesions within the thymic parenchyma. However, on CT, thymic cysts can have increased attenuation values and be mistaken for solid or complex cystic lesions.²¹ Because of this fact, MRI shows a clear advantage over CT, as it more consistently demonstrates the cystic nature of these lesions with better characterization of the cyst contents.¹⁶ Typically, thymic cysts are hypointense on T1-weighted imaging, although T1 signal intensity can vary depending on overall proteinaceous content of the cyst fluid, that is, simple fluid versus hemorrhagic or

proteinaceous fluid. Thymic cysts are always T2 hyperintense, although the degree of hyperintensity is variable. Comparison of unenhanced and enhanced images definitively characterizes the cystic nature of these lesions demonstrating the lack of internal enhancement, a clear advantage over CT, which would require unenhanced and enhanced CT images, doubling the radiation dose given to the patient.¹⁶

Lymphatic Malformation (LMs): LMs result from congenital maldevelopment of the lymphatic channels resulting in a lymph-containing multicystic mass. Although they may occur anywhere in the body, they most commonly affect the axilla, cervicofacial region, presacral area, and the retroperitoneum. Intrathoracic LMs are rare, comprising only 1% of cases,⁶² with the prevascular mediastinum most often affected. As a rule, they do not respect fascial/spatial boundaries.

On CR, LMs appear as large soft tissue masses, which may extend into or extend from the base of the neck or the adjacent chest wall. Cross-sectional imaging (Fig. 10) is nearly uniformly used, as the CR appearance is nonspecific. In a very young child, US may be used and demonstrates a heterogenous, multicystic mass with no vascular flow within the cystic components on Doppler. In most cases, however, CT or MRI is performed, as US may be limited in defining the overall mass extent. MRI, particularly when performed using newer motion correction sequences, exquisitely demonstrates both the cystic and solid components as well as the lesional extent and is the imaging modality of choice. The intracystic contents are most often hyperintense on T2 but may have a variable T1 appearance, depending on protein content or prior hemorrhage. Following gadolinium, the cyst walls may enhance. If prior infection or hemorrhage has occurred, variable internal enhancement may be seen.² Time-resolved MR angiography may be helpful to assess for



FIGURE 10. Newborn with prenatal diagnosis of LM. Axial chest CT image with intravenous contrast demonstrates a well-circumscribed, slightly lobulated mass (arrow) with the center in the visceral mediastinal compartment and extending into the paravertebral compartment consistent with the patient's known LM. Although other large and/or aggressive mediastinal masses can compress or invade into other mediastinal compartments, transapical spread is a hallmark of LMs.

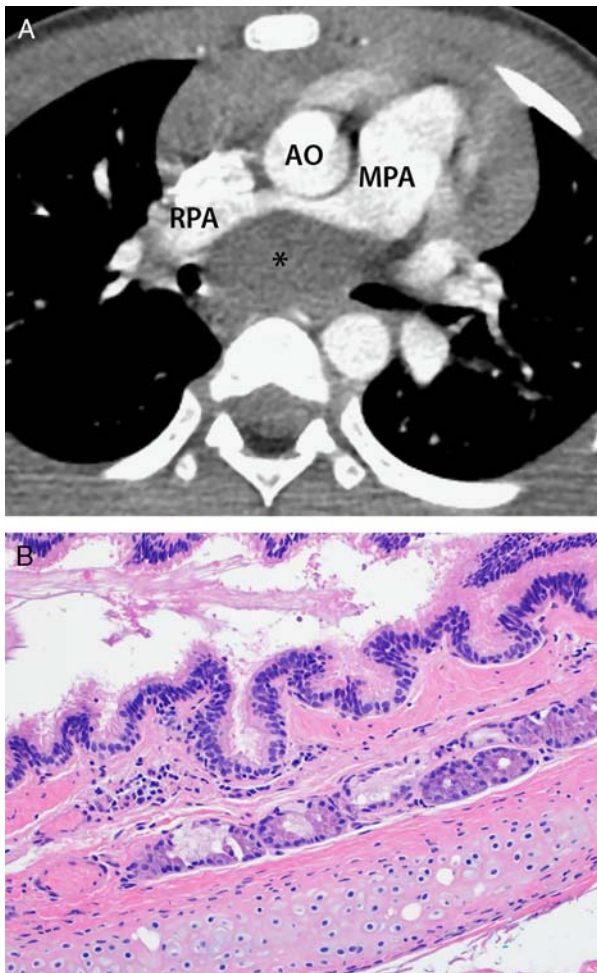


FIGURE 11. 5-year-old boy presenting with a heart murmur. A, Axial contrast-enhanced chest CT image demonstrates a well-defined, nonenhancing fluid attenuation mass (*) within the subcarinal region of the visceral compartment consistent with a foregut duplication cyst. There is associated mass effect on the proximal right pulmonary artery (RPA). Of note, MRI is superior to CT for the evaluation of foregut duplication cysts as hyperdense cystic contents may make these lesions appear solid on CT imaging alone. B, High-magnification histologic specimen showing ciliated respiratory mucosal lining with bronchial glands and cartilage, characteristic of bronchogenic cyst. AO indicates aorta; MPA, main pulmonary artery.

a concurrent venous or arterial component. Similarly, on CT, LMs appear as mostly cystic transapical masses, which may infiltrate around and compress normal mediastinal structures.

Visceral Compartment Masses

Foregut Duplication Cysts (FDCs)

Resulting from embryonic foregut malformation, FDC are divided into 3 main types on the basis of histologic analysis, for example, bronchogenic, esophageal, and neurenteric cysts. FDCs are the most common primary visceral compartment mass, the most common mediastinal cystic mass, and represent 11% of pediatric and 20% of adult mediastinal masses.^{1,52,63} Few imaging features are helpful in differentiating between the types of FDCs with 1

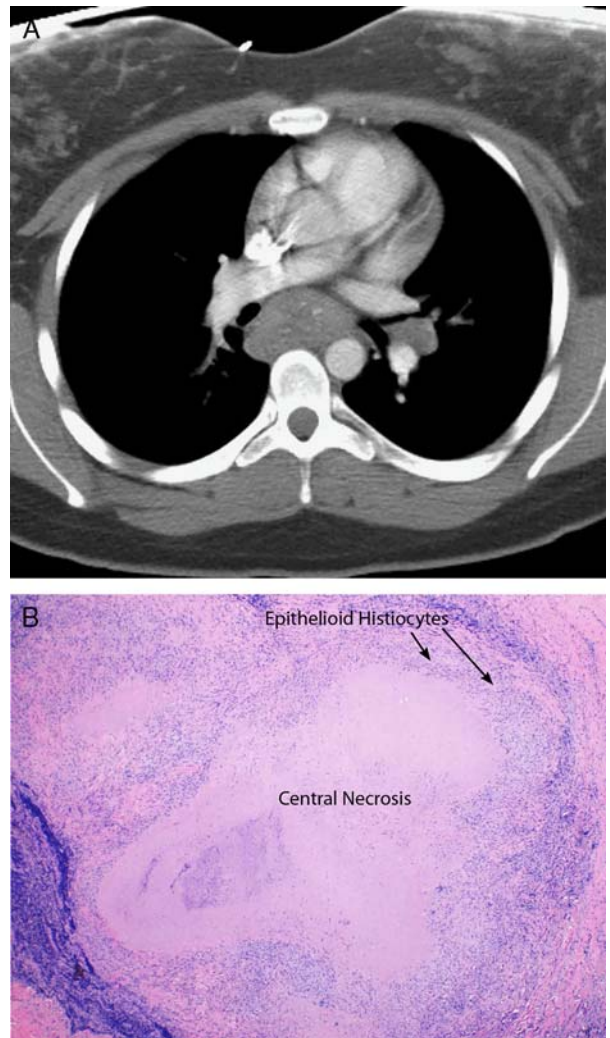


FIGURE 12. 24-year-old woman with dysphagia. A, Contrast-enhanced axial chest CT image demonstrates enlarged subcarinal and left hilar lymph nodes. B, Lymphoid tissue with necrotizing granulomatous inflammation showing central necrosis with a rim of epithelioid histiocytes and rare fungal organisms consistent with histoplasmosis.

exception; the presence of a vertebral cleft with a visceral compartment lesion is pathognomonic of a neurenteric cyst.

On CR, FDCs appear as an oval or rounded, smoothly margined soft tissue mass. On CT and MRI, they are well-margined cystic lesions with minimal to no cyst wall enhancement in uncomplicated cases (Fig. 11). In 50% of cases, the cyst contents are uniformly hyperintense on T2-weighted images and measure at or near 0 HU on CT, consistent with simple fluid.² If infection or intracystic hemorrhage has occurred, the intracystic contents become more proteinaceous and increased in attenuation and may be confused for other mediastinal masses. Accurate localization to the visceral compartment may be helpful for correct diagnosis. If CT remains indeterminate, MRI is particularly helpful as the contents may be hyperintense on pregadolinium T1-weighted images or fluid-fluid levels may be demonstrated. In addition, with prior infection, the cyst walls may become thickened and irregular with more robust enhancement.

Infectious Visceral Compartment Masses

Granulomatous infection, from histoplasmosis or mycobacterial tuberculosis may result in fibrosing mediastinitis, a mass-like proliferation of fibrous tissue and collagen.^{64,65} This mass-like lesion may be highly infiltrative and aggressive-appearing, surrounding and narrowing other mediastinal structures, with affected patients presenting with dysphagia, respiratory distress, and neck and facial swelling.

Fibrosing mediastinitis generally presents as a paratracheal or subcarinal soft tissue mass on CR. Cross-sectional imaging, particularly CT, is helpful in further defining the extent with categorization into diffuse or focal types (Fig. 12).⁶⁶ Focal fibrosing mediastinitis calcifies in 63% of patients and presents as a subcarinal, hilar, or paratracheal soft tissue mass.⁶⁶ In contrast, diffuse fibrosing mediastinitis almost always calcifies and appears as an aggressive, infiltrative soft tissue mass, which may extend to involve multiple mediastinal compartments, surrounding and compressing multiple normal structures.

Neoplastic Visceral Mediastinal Masses

Lymphoma: Although lymphoma most commonly involves the prevascular compartment, it can involve the visceral compartment either by contiguous spread from the prevascular compartment or as a focus of primary visceral compartment involvement. Imaging features are similar to that seen with prevascular lymphoma and include a large conglomerated mass displacing and compressing normal adjacent structures or individual, often bulky lymphadenopathy. Generally, CR is performed first followed by PET/CT for staging and treatment response assessment. However, as above, MRI likely plays an increased role in mediastinal lymphoma.

Midline NUT Tumor: Nuclear protein in testis (NUT) midline carcinoma is a rare, highly aggressive carcinoma resulting from chromosomal rearrangement of the NUT, located on chromosome 15q14. This translocation results in a BRAD4-NUT fusion oncogene.⁶⁷⁻⁶⁹ NUT midline carcinoma most commonly occurs in adolescents and young adults originating in a midline body location, primarily the head, neck, and mediastinum.⁷⁰

Imaging findings of mediastinal NUT midline carcinoma are nonspecific, with relatively little reported in the imaging literature describing these lesions. CR appearance depends on the mass extent ranging from a focal mass within the visceral compartment to complete hemithorax opacification.⁶⁹ Of the cases reported in the literature, NUT midline carcinoma appears on CT as a low-density infiltrative mass with heterogeneous enhancement. Infiltration and/or compression of adjacent mediastinal structures, intralesional calcification, and internal necrosis have also been described.⁶⁷⁻⁶⁹ MRI features correlate with those of CT with diffuse heterogeneity, predominantly T1 hypointensity, and hyperintensity on T2 with heterogeneous enhancement.⁶⁷ PET/CT evaluation has been described with the tumor being FDG avid except in areas of necrosis. FDG avidity has also been found to correlate well with clinical status and tumor burden on CT—that is, serial increased FDG avidity correlates with tumor progression.^{67,69}

Metastatic Disease: Visceral compartment metastatic disease primarily involves spread from locoregional and distant disease to the mediastinal lymph nodes. In children, no defined size criteria has been established to differentiate pathologically enlarged from normal-sized lymph nodes, although some authors argue that any mediastinal lymph

node visualizable on CT should be considered abnormal in children.⁷¹ Nevertheless, newer standard anatomic response criteria assign lymph nodes as pathologically enlarged if the short-axis dimension measures ≥ 10 mm, regardless of age. In children, the most common metastatic disease to the visceral compartment lymph nodes outside of lymphoma are Wilms tumor, Ewing sarcoma, and osteosarcoma. In contrast, the most common adult metastasis is from lung malignancy such as small cell lung cancer.

CR findings vary from normal to a lobulated soft tissue mass within the visceral compartment. For further evaluation, CT or PET/CT in the case of known malignancy is most often performed next and demonstrates single to multiple enlarged visceral lymph nodes with FDG avidity greater than blood pool. Similar to lymphoma, MRI will likely play an increased role in metastatic lymph node imaging. In cases of osteosarcoma, calcifications may be seen on CT in metastatic lesions in chest.

Pitfalls

Pseudoaneurysm: In contrast to true thoracic aortic aneurysms, which contain all 3 layers of the aortic wall, thoracic aortic pseudoaneurysms contain <3 layers and are bounded peripherally by the adventia or periaortia soft tissues.⁷² Most commonly, they result from prior cardiac surgery.^{72,73} In those posttraumatic patients who reach the hospital, the aortic isthmus represents the site of injury in 90%. In patients who survive, 2.5% will develop chronic aortic pseudoaneurysm, which may rupture years after injury.^{72,74,75} A large portion of chronic aortic pseudoaneurysm may present later in life on imaging for an alternative reason. In these situations, they can simulate a mediastinal mass in any of the spaces that they are located on.

On CR, chronic pseudoaneurysms appear as focal soft tissue masses, which may displace adjacent vascular structures (Fig. 13A). Thrombus or calcification may be seen and can simulate calcifications associated with teratomas.^{72,76} MDCT demonstrates continuity with the thoracic aorta. The pseudoaneurysm appears as a focal aortic dilatation or diverticulum with internal contrast enhancement similar to the adjacent normal aorta (Figs. 13B, C). Similarly, MR angiography with either time of flight or postgadolinium sequences has a similar appearance to that of CT but is often not used in the acute setting.

Other Vascular Lesions: Although the heart and pericardium are included within the visceral compartment, a full discussion of both vascular and nonvascular lesions of the heart and pericardium is beyond the scope of this review. Multiple lesions including coronary artery and cardiac sinus abnormalities, cardiac structural abnormalities, pericardial cysts, pericardial sleeve variants, and true cardiac neoplasms can present as focal visceral compartment masses.

Paravertebral Mediastinal Masses

Neurogenic Tumors

Sympathetic Chain Ganglion Origin Tumors: Thirty-four percent of pediatric mediastinal masses are located in the paravertebral compartment, with 88% to 90% being neurogenic in origin.^{1,2} In adults, 20% of mediastinal masses have a neurogenic origin.⁶³ Approximately 80% of these neurogenic tumors arise in the paravertebral sympathetic chain ganglion. In children, most are neuroblastomas (Fig. 14) with the remainder composed of ganglioneuroblastomas (Fig. 15A) and ganglioneuromas (Fig. 15B). These tumors form a disease

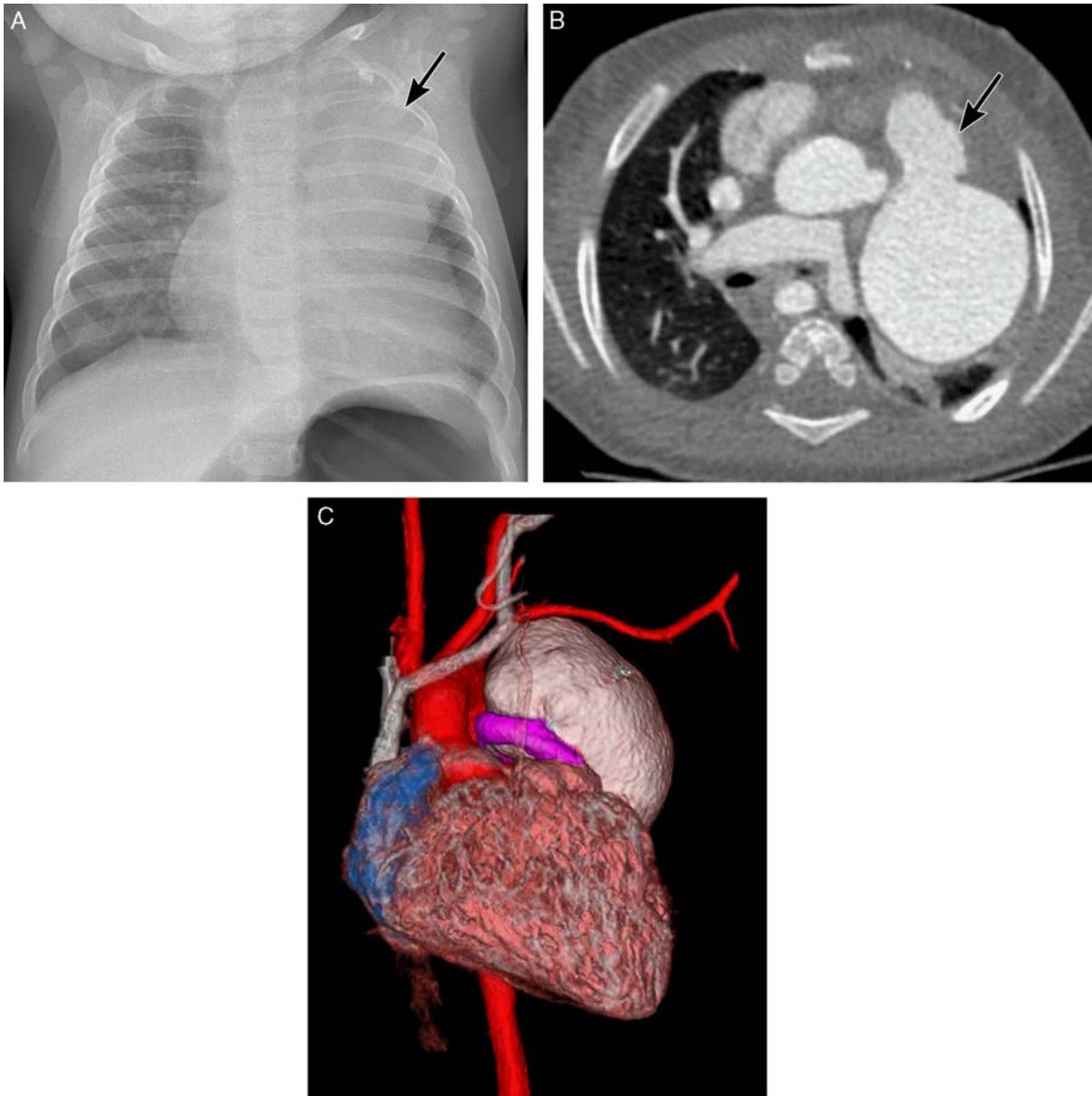


FIGURE 13. 5-month-old girl with cough. A, Frontal CR demonstrates widening of the mediastinum and abnormal mediastinal contour (arrow). The patient was diagnosed first with an anterior mediastinal mass likely due to lymphoma on the emergency room visit. Further evaluation of the patient’s history revealed prior cardiac surgery including placement of a right ventricle to pulmonary artery conduit for truncus arteriosus repair. B, Axial chest CT angiographic image reveals a large pseudoaneurysm arising from the right ventricle conduit (arrow) and causing compression on the right branch pulmonary artery. C, Volume-rendered 3-dimensional reformatted image shows a large pseudoaneurysm (pink structure) from the main pulmonary artery conduit. Urgent surgery was performed. Although vascular lesions are occasionally omitted from the mediastinal mass differential diagnosis, they represent a potential pitfall to the unaware radiologist. [full color online](#)

spectrum with neuroblastomas having the least cellular differentiation and being the most malignant, whereas gangliogliomas have the most cellular differentiation and are the least aggressive. Imaging is insensitive for differentiation between the 3 types, although older patients or incidental detection suggests lesions on the more benign spectrum.

Calcifications are seen in up to 30% of tumors on CRs with the mass appearing as a well-defined soft tissue opacity in the paravertebral compartment.² Rib and vertebral body erosions, neuroforaminal widening, and intercostal splay-

ing may also be demonstrated. On CT, they appear as well-defined, lenticular-shaped paravertebral masses with curvilinear or punctate calcifications (Fig. 14). They may be uniformly homogenous to very heterogenous depending on the presence and degree of intratumoral necrosis. Although demonstrable on CT, neuroforaminal invasion and intraspinal canal extension is shown to best advantage on MRI with the mass being hyperintense on T2-weighted images (Fig. 15A). Rapid enhancement occurs after contrast material administration, reflecting their highly vascular nature.

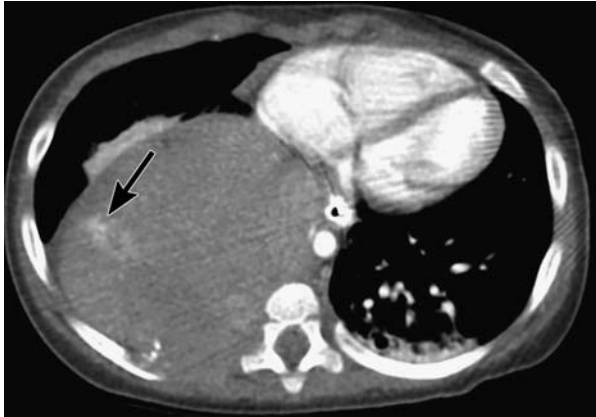


FIGURE 14. Neuroblastoma in an 8-month-old boy. Axial contrast-enhanced chest CT demonstrates a large paravertebral mass with amorphous internal calcifications (arrow) and compression and displacement of the heart with esophageal and aortic displacement. There is subtle invasion into the spinal canal better demonstrated on follow-up MRI (not shown). As this mass demonstrates, large mediastinal masses may be difficult to localize. However, evaluation of normal structure displacement readily demonstrates that this lesion originated in the paravertebral compartment.

MIBG imaging is particularly useful in the workup and treatment evaluation of these lesions and should be performed before surgical or medical intervention. On planar and single-photon emission CT MIBG imaging, neuroblastomas show abnormal radiotracer uptake within the paravertebral compartment. It is important to note before treatment whether neuroblastomas are MIBG positive. If a lesion is responsive to chemotherapy, the tumor will become MIBG negative as it involutes. In unresponsive or recurrent neuroblastoma, if the tumor is initially positive and subsequently becomes nonavid for MIBG, this denotes a poor prognostic sign.

Nerve Root Origin Tumors: Thoracic nerve root origin tumors, for example, schwannomas and neurofibromas, are composed of myxoid stroma and spindle cells and arise from intercostal nerves within the paravertebral compartment. They are less common in children relative to sympathetic chain ganglion tumors. Neurofibromatosis type 1 should be suspected in the setting of plexiform neurofibromas. Very rarely, malignant peripheral nerve sheath tumors (PNSTs) may arise de novo or from existing plexiform neurofibromas and schwannomas.²

PNSTs appear on CR as elliptical or rounded, well-defined soft tissue masses within the paravertebral compartment (Fig. 16). They may cause osseous remodeling of the vertebral bodies and ribs as they grow along nerve roots.⁶³ The “ribbon rib” sign is a classic radiographic finding often associated with neurofibromas when significant rib erosions develop.

The CT appearance of schwannomas and neurofibromas is similar. On CT, schwannomas appear as round, well-defined lesions with smooth margins and are isodense or hypodense to the adjacent chest wall musculature. They have a variable enhancement pattern after contrast material administration including multiple hypodense or cystic areas, diffuse heterogeneous enhancement, peripheral enhancement with central hypodensity, and central enhancement with peripheral hypodensity. Similarly, neurofibromas appear as

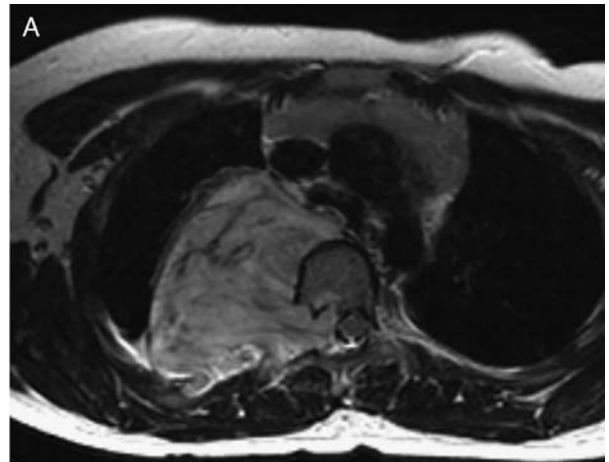


FIGURE 15. A, 9-year-old boy with ganglioneuroblastoma. Axial turbo spin-echo T2-weighted image without fat saturation demonstrates a large, heterogeneous but mostly hyperintense, right paravertebral mass with invasion of the adjacent neuroforamen and displacement of the thecal sac. Notably, MRI is superior to all other imaging modalities for demonstrating the invasion of the spinal canal and should be performed in cases of paravertebral compartment masses. B, 6-year-old girl presenting with fever and vomiting. Axial contrast-enhanced chest CT shows a well-defined left paravertebral soft tissue mass (arrow) consistent with a pathologically proven ganglioneuroma.

smooth, oval or rounded paraspinal masses displacing adjacent structures and often extending along the margins of the ribs. Like schwannomas, neurofibromas are generally isodense to muscle. They show variable enhancement after contrast material administration.⁷⁷

In contrast to CT, MRI is better able to characterize and differentiate between schwannomas and neurofibromas. On T1-weighted imaging, schwannomas demonstrated T1 signal intensity that is equal to or greater than chest wall musculature. Similarly, neurofibromas have uniform low T1 signal intensity equal to muscle. T2 signal intensity is helpful in differentiating the 2, with neurofibromas having peripheral, rim-like T2 hyperintensity with low signal centrally giving the classic “target” sign. In

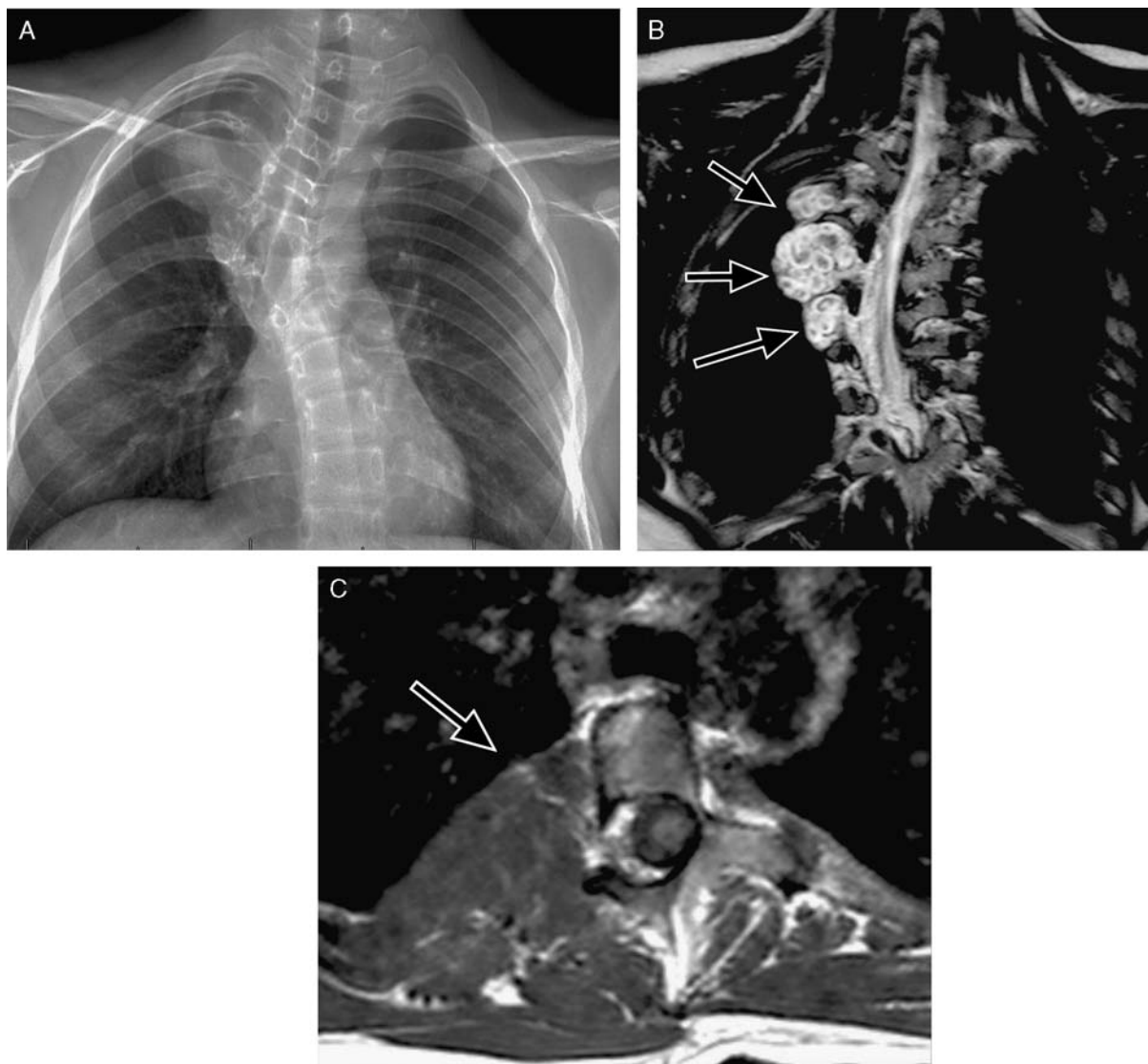


FIGURE 16. Posterior mediastinal mass in an 11-year-old girl with scoliosis and segmentation anomaly of the spine. A, Note the extension of soft tissue opacity above the clavicle on the CR suggesting posterior spinal mass (cervico-thoracic sign). B and C, Subsequent MRI shows paraspinal masses (arrows), which are high signal on the T2-weighted image (B) at the level of neural foramina with “target appearance” and are low signal (arrow) on the T1-weighted image (C) consistent with neurofibromatosis.

contrast, T2 signal intensity is often heterogenous in schwannomas with intermediate to high signal compared with adjacent fat. Both demonstrate avid enhancement after contrast material administration.⁷⁷

Malignant PNSTs have a more aggressive appearance on imaging with areas of necrosis, variable enhancement, and intraspinal extension. Other features that help suggest malignant rather than benign PNSTs are rapid growth over serial imaging, pleural effusions, metastatic pulmonary nodules, and local invasion.^{2,77} In addition, PET also may be helpful in distinguishing malignant degeneration of a benign PNST in the setting of type 1 neurofibromatosis.⁷⁸

Miscellaneous

Posterior Diaphragmatic Hernia: The diaphragm is the primary muscle of respiration, with the septum transversum forming its ventral component during the third to fifth week

of gestation.⁷⁹ The septum transversum progressively extends posteriorly to fuse with the foregut mesentery and the thoracic wall muscles to form the posteromedial and posterolateral diaphragmatic components, respectively. The Bochdalek (pleuroperitoneal) foramina, located posterolaterally, is the last to close.⁷⁹ Both congenital and acquired diaphragmatic hernias can simulate a paravertebral compartment mass, particularly when large, and must be considered in the differential diagnosis.

Congenital diaphragmatic hernias have a prevalence ranging from 1.7 to 5.7/10,000 live births, with the most common being a Bochdalek hernia.⁷⁹⁻⁸² Eighty percent of Bochdalek hernias are left sided, and rarely are they bilateral.⁷⁹ Most present during early childhood, especially if large, because of pulmonary hypoplasia. However, small congenital diaphragmatic hernias may remain asymptomatic and be found in adulthood during which they are incidentally detected.

Acquired diaphragmatic hernias may be posttraumatic, most commonly left sided, or iatrogenic, in cases in which the diaphragm is injured during thoraco-abdominal surgery.⁷⁹ Both may occur anywhere along the age spectrum.

CR is generally the first imaging study performed postnatally and in older children and adults. Posterior diaphragmatic hernias appear as a soft tissue mass without or with intestinal gas. In the case of traumatic diaphragmatic hernia, associated hemopneumothorax and rib fractures can be seen.⁷⁹ CT is usually the next study performed and, in most cases, clearly visualizes the hernia site and herniated organs. Multiplanar reformations and 3-dimensional reconstructions help improve depiction of the diaphragmatic discontinuity as well as any associated findings such as bowel constriction or obstruction. MRI is typically not utilized in the postnatal period because of its sensitivity to motion artifact and need for sedation in young children. However, prenatally, MRI has increasingly been used to confirm the diagnosis by discriminating lung lesions, which may simulate a diaphragmatic hernia, while at the same time evaluating for associated anomalies and providing detailed thoracic anatomy.⁸³ Depending on the gestational age, herniated bowel can range from T1 hypointense to T1 hyperintense, reflecting the degree of meconium. T1-weighted images are also useful in verifying the liver location and have been shown to be more accurate than US for liver herniation.^{83,84} In addition, although no single marker is absolutely predictive of postnatal mortality, the degree of pulmonary hypoplasia is an important determinant of patient survival. In this setting, MRI has been shown to offer a better predictive value as compared with US and is progressively becoming the imaging modality of choice.⁸⁵

Extramedullary Hematopoiesis: In patients with ineffective erythropoiesis, for example, sickle cell anemia and thalassemia, hematopoietic cells may proliferate outside of the bone marrow leading to “tumor-like” formations.^{86,87} Although a multitude of sites has been described for extramedullary hematopoiesis, the paravertebral mediastinum is one of the most common, and paraosseous extramedullary hematopoiesis is the most common intrathoracic manifestation.⁸⁷ In this location, extramedullary hematopoiesis may be confused for other paravertebral masses; thus, imaging plays a crucial role along with patient history in evaluation and differentiation.

CR demonstrates a smooth or lobulated, well-defined paraspinal mass with sizes ranging from small isolated foci to extensive and bilateral masses. Rib expansion and inner cortex permeative erosions are also a common radiographic finding, particularly in β -thalassemia.^{88,89} On CT, extramedullary hematopoiesis appears as a sharply defined paraspinal mass with exuberant contrast enhancement. Iron or fatty deposition in long-standing lesions as well as internal calcification have been reported.^{87,88,90} MRI findings are nonspecific but can be suggestive of the diagnosis, particularly when bilateral paravertebral masses are present in the setting of diffuse low signal in the vertebral bodies, corresponding to iron deposition.⁸⁸ As extramedullary hematopoiesis may also extend into the spinal canal, MRI has supplanted all other imaging methods for the diagnosis and follow-up of associated cord compression.⁸⁶

CONCLUSIONS

Imaging plays a vital role in the evaluation of mediastinal masses in both children and adults. CR is often the

first modality utilized in all age groups. Following radiographs, CT or MRI is often used to localize and further characterize mediastinal masses, in select cases yielding a definitive diagnosis. A new CT-based classification system has been recently reported and should be incorporated into our imaging interpretation scheme. Knowledge of this system, as well as the strengths and weaknesses of each imaging modality and the imaging characteristics for each lesion, is crucial as it helps in establishing a cost-effective imaging plan, guiding diagnosis and treatment decisions and ultimately leading to improved patient outcomes.

REFERENCES

1. Lee EY. Evaluation of non-vascular mediastinal masses in infants and children: an evidence-based practical approach. *Pediatr Radiol.* 2009;39(suppl 2):S184–S190.
2. Ranganath SH, Lee EY, Restrepo R, et al. Mediastinal masses in children. *Am J Roentgenol.* 2012;198:W197–W216.
3. Fujimoto K, Hara M, Tomiyama N, et al. Proposal for a new mediastinal compartment classification of transverse plane images according to the Japanese Association for Research on the Thymus (JART) General Rules for the Study of Mediastinal Tumors. *Oncol Rep.* 2014;31:565–572.
4. Carter BW, Tomiyama N, Bhora FY, et al. A modern definition of mediastinal compartments. *J Thorac Oncol.* 2014; 9:S97–S101.
5. Kim OH, Kim WS, Kim MJ, et al. US in the diagnosis of pediatric chest diseases. *Radiographics.* 2000;20:653–671.
6. Graeber GM, Shriver CD, Albus RA, et al. The use of computed tomography in the evaluation of mediastinal masses. *J Thorac Cardiovasc Surg.* 1986;91:662–666.
7. Siegel MJ, Sagel SS, Reed K. The value of computed tomography in the diagnosis and management of pediatric mediastinal abnormalities. *Radiology.* 1982;142:149–155.
8. Yanagawa M, Gyobu T, Leung AN, et al. Ultra-low-dose CT of the lung: effect of iterative reconstruction techniques on image quality. *Acad Radiol.* 2014;21:695–703.
9. Gawande RS, Khurana A, Messing S, et al. Differentiation of normal thymus from anterior mediastinal lymphoma and lymphoma recurrence at pediatric PET/CT. *Radiology.* 2012; 262:613–622.
10. Hudson MM, Krasin MJ, Kaste SC. PET imaging in pediatric Hodgkin's lymphoma. *Pediatr Radiol.* 2004;34:190–198.
11. Shankar A, Fiumara F, Pinkerton R. Role of FDG PET in the management of childhood lymphomas—case proven or is the jury still out? *Eur J Cancer.* 2008;44:663–673.
12. Montravers F, McNamara D, Landman-Parker J, et al. [(18)F]FDG in childhood lymphoma: clinical utility and impact on management. *Eur J Nucl Med Mol Imaging.* 2002;29:1155–1165.
13. Wegner EA, Barrington SF, Kingston JE, et al. The impact of PET scanning on management of paediatric oncology patients. *Eur J Nucl Med Mol Imaging.* 2005;32:23–30.
14. Depas G, De Barys C, Jerusalem G, et al. 18F-FDG PET in children with lymphomas. *Eur J Nucl Med Mol Imaging.* 2005; 32:31–38.
15. Kushner BH. Neuroblastoma: a disease requiring a multitude of imaging studies. *J Nucl Med.* 2004;45:1172–1188.
16. Ackman JB, Wu CC. MRI of the thymus. *Am J Roentgenol.* 2011;197:W15–W20.
17. Costa NS, Laor T, Donnelly LF. Superior cervical extension of the thymus: a normal finding that should not be mistaken for a mass. *Radiology.* 2010;256:238–242.
18. Mizuno T, Hashimoto T, Masaoka A, et al. Thymic follicular hyperplasia manifested as an anterior mediastinal mass. *Surg Today.* 1997;27:275–277.
19. Nasseri F, Eftekhari F. Clinical and radiologic review of the normal and abnormal thymus: pearls and pitfalls. *Radiographics.* 2010;30:413–428.

20. Araki T, Sholl LM, Gerbaudo VH, et al. Imaging characteristics of pathologically proven thymic hyperplasia: identifying features that can differentiate true from lymphoid hyperplasia. *Am J Roentgenol.* 2014;202:471–478.
21. Ackman JB, Verzosa S, Kovach AE, et al. High rate of unnecessary thymectomy and its cause. Can computed tomography distinguish thymoma, lymphoma, thymic hyperplasia, and thymic cysts? *Eur J Radiol.* 2015;84:524–533.
22. Inaoka T, Takahashi K, Mineta M, et al. Thymic hyperplasia and thymus gland tumors: differentiation with chemical shift MR imaging. *Radiology.* 2007;243:869–876.
23. Qu YJ, Liu GB, Shi HS, et al. Preoperative CT findings of thymoma are correlated with postoperative Masaoka clinical stage. *Acad Radiol.* 2013;20:66–72.
24. Detterbeck FC, Nicholson AG, Kondo K, et al. The Masaoka-Koga stage classification for thymic malignancies: clarification and definition of terms. *J Thorac Oncol.* 2011;6: S1710–S1716.
25. Masaoka A. Staging system of thymoma. *J Thorac Oncol.* 2010;5:S304–S312.
26. Detterbeck FC, Asamura H, Crowley J, et al. The IASLC/ITMIG thymic malignancies staging project: development of a stage classification for thymic malignancies. *J Thorac Oncol.* 2013;8:1467–1473.
27. Nason LK, Walker CM, McNeeley MF, et al. Imaging of the diaphragm: anatomy and function. *Radiographics.* 2012;32: E51–E70.
28. Restrepo CS, Pandit M, Rojas IC, et al. Imaging findings of expansile lesions of the thymus. *Curr Probl Diagn Radiol.* 2005;34:22–34.
29. Nishino M, Ashiku SK, Kocher ON, et al. The thymus: a comprehensive review. *Radiographics.* 2006;26:335–348.
30. Gartner LA, Voorhess ML. Adrenocorticotropic hormone—producing thymic carcinoid in a teenager. *Cancer.* 1993;71: 106–111.
31. Economopoulos GC, Lewis JW Jr, Lee MW, et al. Carcinoid tumors of the thymus. *Ann Thorac Surg.* 1990;50:58–61.
32. Wick MR, Scott RE, Li CY, et al. Carcinoid tumor of the thymus: a clinicopathologic report of seven cases with a review of the literature. *Mayo Clin Proc.* 1980;55:246–254.
33. Lowenthal RM, Gumpel JM, Kreel L, et al. Carcinoid tumour of the thymus with systemic manifestations: a radiological and pathological study. *Thorax.* 1974;29:553–558.
34. Rosai J, Higa E. Mediastinal endocrine neoplasm, of probable thymic origin, related to carcinoid tumor. Clinicopathologic study of 8 cases. *Cancer.* 1972;29:1061–1074.
35. Sharma P, Singhal A, Kumar A, et al. Evaluation of thymic tumors with 18F-FDG PET-CT: a pictorial review. *Acta radiol.* 2013;54:14–21.
36. Syrios J, Diamantis N, Fergadis E, et al. Advances in thymic carcinoma diagnosis and treatment: a review of literature. *Med Oncol.* 2014;31:44.
37. Sadohara J, Fujimoto K, Muller NL, et al. Thymic epithelial tumors: comparison of CT and MR imaging findings of low-risk thymomas, high-risk thymomas, and thymic carcinomas. *Eur J Radiol.* 2006;60:70–79.
38. Abdel Razek AA, Khairy M, Nada N, et al. Diffusion-weighted MR imaging in thymic epithelial tumors: correlation with World Health Organization classification and clinical staging. *Radiology.* 2014;273:268–275.
39. Chen X, Xu H, Ni Y, et al. Complete excision of a giant thyroid goiter in posterior mediastinum. *J Cardiothorac Surg.* 2013;8:207.
40. Baron RL, Lee JK, Sagel SS, et al. Computed tomography of the normal thymus. *Radiology.* 1982;142:121–125.
41. Tece PM, Fishman EK, Kuhlman JE. CT evaluation of the anterior mediastinum: spectrum of disease. *Radiographics.* 1994;14:973–990.
42. Mercante G, Gabrielli E, Pedroni C, et al. CT cross-sectional imaging classification system for substernal goiter based on risk factors for an extracervical surgical approach. *Head Neck.* 2011;33:792–799.
43. Hong BW, Mazeh H, Chen H, et al. Routine chest X-ray prior to thyroid surgery: is it always necessary? *World J Surg.* 2012;36:2584–2589.
44. Mastrolia SA, Mandola A, Mazor M, et al. Antenatal diagnosis and treatment of hypothyroid fetal goiter in an euthyroid mother: a case report and review of literature. *J Matern Fetal Neonatal Med.* 2014;8:1–7.
45. Carter BW, Marom EM, Detterbeck FC. Approaching the patient with an anterior mediastinal mass: a guide for clinicians. *J Thorac Oncol.* 2014;9:S102–S109.
46. Mayerhoefer ME, Karanikas G, Kletter K, et al. Evaluation of diffusion-weighted MRI for pretherapeutic assessment and staging of lymphoma: results of a prospective study in 140 patients. *Clin Cancer Res.* 2014;20:2984–2993.
47. Punwani S, Taylor SA, Saad ZZ, et al. Diffusion-weighted MRI of lymphoma: prognostic utility and implications for PET/MRI? *Eur J Nucl Med Mol Imaging.* 2013;40: 373–385.
48. Sakai S, Murayama S, Soeda H, et al. Differential diagnosis between thymoma and non-thymoma by dynamic MR imaging. *Acta radiol.* 2002;43:262–268.
49. Klimstra DS, Moran CA, Perino G, et al. Liposarcoma of the anterior mediastinum and thymus. A clinicopathologic study of 28 cases. *Am J Surg Pathol.* 1995;19:782–791.
50. Munk PL, Lee MJ, Janzen DL, et al. Lipoma and liposarcoma: evaluation using CT and MR imaging. *Am J Roentgenol.* 1997;169:589–594.
51. Eisenstat R, Bruce D, Williams LE, et al. Primary liposarcoma of the mediastinum with coexistent mediastinal lipomatosis. *Am J Roentgenol.* 2000;174:572–573.
52. Williams HJ, Alton HM. Imaging of paediatric mediastinal abnormalities. *Paediatr Respir Rev.* 2003;4:55–66.
53. Billmire DF. Germ cell, mesenchymal, and thymic tumors of the mediastinum. *Semin Pediatr Surg.* 1999;8:85–91.
54. Tian L, Liu LZ, Cui CY, et al. CT findings of primary non-teratomatous germ cell tumors of the mediastinum—a report of 15 cases. *Eur J Radiol.* 2012;81:1057–1061.
55. Merten DF. Diagnostic imaging of mediastinal masses in children. *Am J Roentgenol.* 1992;158:825–832.
56. Meza MP, Benson M, Slovis TL. Imaging of mediastinal masses in children. *Radiol Clin North Am.* 1993;31: 583–604.
57. Moeller KH, Rosado-de-Christenson ML, Templeton PA. Mediastinal mature teratoma: imaging features. *Am J Roentgenol.* 1997;169:985–990.
58. Rosado-de-Christenson ML, Templeton PA, Moran CA. From the archives of the AFIP. Mediastinal germ cell tumors: radiologic and pathologic correlation. *Radiographics.* 1992; 12:1013–1030.
59. Tomiyama N, Honda O, Tsubamoto M, et al. Anterior mediastinal tumors: diagnostic accuracy of CT and MRI. *Eur J Radiol.* 2009;69:280–288.
60. Oldenburg J, Fossa SD, Nuvér J, et al. Testicular seminoma and non-seminoma: ESMO Clinical Practice Guidelines for diagnosis, treatment and follow-up. *Ann Oncol.* 2013;24 (suppl 6):vi125–vi132.
61. Chou SH, Prabhu SJ, Crothers K, et al. Thoracic diseases associated with HIV infection in the era of antiretroviral therapy: clinical and imaging findings. *Radiographics.* 2014;34:895–911.
62. Wildi SM, Hoda RS, Fickling W, et al. Diagnosis of benign cysts of the mediastinum: the role and risks of EUS and FNA. *Gastrointest Endosc.* 2003;58:362–368.
63. Strollo DC, Rosado-de-Christenson ML, Jett JR. Primary mediastinal tumors: part II. Tumors of the middle and posterior mediastinum. *Chest.* 1997;112:1344–1357.
64. Devaraj A, Griffin N, Nicholson AG, et al. Computed tomography findings in fibrosing mediastinitis. *Clin Radiol.* 2007;62:781–786.
65. Rodriguez E, Soler R, Pombo F, et al. Fibrosing mediastinitis: CT and MR findings. *Clin Radiol.* 1998;53:907–910.
66. Sherrick AD, Brown LR, Harms GF, et al. The radiographic findings of fibrosing mediastinitis. *Chest.* 1994;106:484–489.

67. Polsani A, Braithwaite KA, Alazraki AL, et al. NUT midline carcinoma: an imaging case series and review of literature. *Pediatr Radiol*. 2012;42:205–210.
68. Nelson BA, Lee EY, French CA, et al. BRD4-NUT carcinoma of the mediastinum in a pediatric patient: multidetector computed tomography imaging findings. *J Thorac Imaging*. 2010;25:W93–W96.
69. Rosenbaum DG, Teruya-Feldstein J, Price AP, et al. Radiologic features of NUT midline carcinoma in an adolescent. *Pediatr Radiol*. 2012;42:249–252.
70. Niederkoher RD, Cameron MJ, French CA. FDG PET/CT imaging of NUT midline carcinoma. *Clin Nucl Med*. 2011;36:e124–e126.
71. Andronikou S. Pathological correlation of CT-detected mediastinal lymphadenopathy in children: the lack of size threshold criteria for abnormality. *Pediatr Radiol*. 2002;32:912.
72. Agarwal PP, Chughtai A, Matzinger FR, et al. Multidetector CT of thoracic aortic aneurysms. *Radiographics*. 2009;29:537–552.
73. Marcano L, Naranjo A, Diaz F, et al. Ascending aortic pseudoaneurysm after aortic valve replacement with root enlargement in a pediatric patient. *Pediatr Radiol*. 2011;32:853–854.
74. Posniak HV, Olson MC, Demos TC, et al. CT of thoracic aortic aneurysms. *Radiographics*. 1990;10:839–855.
75. Lande A, Berkmen YM. Aortitis: pathologic, clinical and arteriographic review. *Radiol Clin North Am*. 1976;14:219–240.
76. Beslic S, Beslic N, Beslic S, et al. Diagnostic imaging of traumatic pseudoaneurysm of the thoracic aorta. *Radiol Oncol*. 2010;44:158–163.
77. O'Sullivan P, O'Dwyer H, Flint J, et al. Soft tissue tumours and mass-like lesions of the chest wall: a pictorial review of CT and MR findings. *Br J Radiol*. 2007;80:574–580.
78. Bredella MA, Torriani M, Hornicek F, et al. Value of PET in the assessment of patients with neurofibromatosis type 1. *Am J Roentgenol*. 2007;189:928–935.
79. Eren S, Ciris F. Diaphragmatic hernia: diagnostic approaches with review of the literature. *Eur J Radiol*. 2005;54:448–459.
80. Garne E, Haeusler M, Barisic I, et al. Congenital diaphragmatic hernia: evaluation of prenatal diagnosis in 20 European regions. *Ultrasound Obstet Gynecol*. 2002;19:329–333.
81. Harrison MR, de Lorimier AA. Congenital diaphragmatic hernia. *Surg Clin North Am*. 1981;61:1023–1035.
82. Torfs CP, Curry CJ, Bateson TF, et al. A population-based study of congenital diaphragmatic hernia. *Teratology*. 1992;46:555–565.
83. Kline-Fath BM. Current advances in prenatal imaging of congenital diaphragmatic [corrected] hernia. *Pediatr Radiol*. 2012;42(suppl 1):S74–S90.
84. Hubbard AM, Crombleholme TM, Adzick NS, et al. Prenatal MRI evaluation of congenital diaphragmatic hernia. *Am J Perinatol*. 1999;16:407–413.
85. Bebbington M, Victoria T, Danzer E, et al. Comparison of ultrasound and magnetic resonance imaging parameters in predicting survival in isolated left-sided congenital diaphragmatic hernia. *Ultrasound Obstet Gynecol*. 2014;43:670–674.
86. Haidar R, Mhaidli H, Taher AT. Paraspinal extramedullary hematopoiesis in patients with thalassemia intermedia. *Eur Spine J*. 2010;19:871–878.
87. Berkmen YM, Zalta BA. Case 126: extramedullary hematopoiesis. *Radiology*. 2007;245:905–908.
88. Georgiades CS, Neyman EG, Francis IR, et al. Typical and atypical presentations of extramedullary hemopoiesis. *Am J Roentgenol*. 2002;179:1239–1243.
89. Tunaci M, Tunaci A, Engin G, et al. Imaging features of thalassemia. *Eur Radiol*. 1999;9:1804–1809.
90. Bolaman Z, Polatli M, Cildag O, et al. Intrathoracic extramedullary hematopoiesis resembling posterior mediastinal tumor. *Am J Med*. 2002;112:739–741.

Questions marked with an asterisk are ABR Self-Assessment Module (SAM) questions. Participants can claim credit for the SAM regardless of the test outcome. Notify the ABR of the SAM completion, or visit the ABR website at www.theabr.org to set up or login to your personal database to record the number of SAMs you completed. The SAM ID number will be printed on the CME certificate for your records. If you wish to include the ID number in your ABR database, contact a MOC Specialist at the ABR office for instruction by calling 520-519-2152.